THE JOURNAL OF PHYSICAL CHEMISTRY B

ARTICLE

pubs.acs.org/JPCB

Signature of Nonadiabatic Transitions on the Pump−Probe Infrared Spectra of a Hydrogen-Bonded Complex Dissolved in a Polar Solvent: A Computational Study

Gabriel Hanna*,‡ and Eitan Geva*,§

‡Department of Chemistry, University of Alberta, Edmonton, Alberta, Canada

§Department of Chemistry, University of Michigan, Ann Arbor, Michigan 48109

ABSTRACT: The mixed quantum-classical Liouville equation provides a unified and self-consistent platform for modeling the spectral signatures of nonequilibrium solvation dynamics, non-Condon effects, and nonadiabatic transitions. These features are demonstrated in this paper in the context of the pump−probe infrared spectra of the hydrogen stretch in a moderately strong hydrogen-bonded complex dissolved in a polar solvent. Particular emphasis is put on incorporating nonadiabatic transitions and accounting for their unique spectral signature.

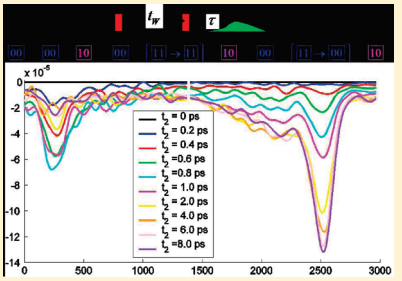

I. INTRODUCTION

A variety of powerful optical probes of the structure and dynamics of molecular systems have been introduced over the last few decades.[1−7] Consequently, numerous theoretical approaches have been introduced in order to model the spectra and interpret them in terms of the underlying molecular structure and dynamics.[1,6,8−10] Modeling the spectra in the case of complex condensed phase systems usually relies on a mixed quantum-classical methodology where the typically small subset of photoactive degrees of freedom (DOF), that is, the *chromophore*, are treated quantum-mechanically while the remaining photoinactive DOF, that is, the *bath*, are treated in a classical-like manner.[1,11−13] It is also commonly assumed that the molecular dynamics (MD) of the bath DOF is governed by the adiabatic potential energy surface (PES) that corresponds to the chromophore's ground state. However, this approach can only be justified when the ground and excited PESs are similar, for example, in the limit of weak chromophore−bath coupling, or when the spectra are inherently insensitive to the bath dynamics, for example, in the limit of inhomogeneous broadening. In cases where these assumptions are not valid, one should expect the spectra to also reflect *nonequilibrium* solvation dynamics that take place on the ground and excited PESs, as well as *nonadiabatic transitions* between them.

We have recently proposed[14] calculating linear and nonlinear spectra based on the mixed quantum-classical Liouville (MQCL) equation.[15−30] Unlike the ground state approach, a MQCL-based approach can account for nonequilibrium dynamics on multiple PESs as well as nonadiabatic transitions between them. We have shown that the MQCL-based approach becomes equivalent to the linearized semiclassical (LSC) approach[10,31] in the absence of nonadiabatic transitions. We have also demonstrated its applicability in this case by calculating the one- and two-dimensional infrared spectra of the hydrogen (H) stretch within the framework of the Azzouz−Borgis (AB) model for a moderately strong H-bonded phenol-amine complex dissolved in liquid methyl-chloride.[32] However, the spectral effects of nonadiabatic transitions were not accounted for in ref 14. Thus, the goal of this paper is twofold: (1) develop a feasible MQCL-based scheme for modeling the spectra in the presence of nonadiabatic transitions; (2) use this scheme in order to gain insight into the spectral signatures of nonadiabatic transitions on the pump−probe infrared spectra of the H-stretch in a H-bonded complex dissolved in a polar solvent.

The remainder of this paper is arranged as follows. In section II, we provide a brief review of the MQCL equation in the case of a system driven by a classical radiation field. In section III, we present a formulation of optical response in the presence of nonadiabatic transitions, with emphasis on third-order response, and in particular the pump−probe spectrum, of a two-state system. In section IV, we use the proposed approach to compute the pump−probe spectra of the H-stretch of a H-bonded complex dissolved in a dipolar liquid. We conclude with a summary of the main results in section V.

II. MIXED QUANTUM-CLASSICAL LIOUVILLE DYNAMICS OF A SYSTEM DRIVEN BY A CLASSICAL RADIATION FIELD

Consider a system driven by a classical radiation field, whose mixed quantum-classical Hamiltonian is explicitly

Special Issue: Shaul Mukamel Festschrift

Received: July 3, 2010
Revised: August 11, 2010
Published: September 20, 2010

time-dependent and given by:

$$\hat{H}(t) = \sum_{j=1}^{n} \frac{\hat{\mathbf{p}}_j^{\,2}}{2m_j} + \sum_{J=1}^{N} \frac{\mathbf{P}_J^{\,2}}{2M_J} + V(\hat{\mathbf{r}}, \mathbf{R}) + W(\hat{\mathbf{r}}, t)$$

$$\equiv \hat{H} + \hat{W}(\hat{\mathbf{r}}, t) \quad (1)$$

Here, $\{m_1,.. .,m_n\}$, $\hat{\mathbf{r}} = (\hat{\mathbf{r}}_1,.. .,\hat{\mathbf{r}}_n)$, and $\hat{\mathbf{p}} = (\hat{\mathbf{p}}_1,.. .,\hat{\mathbf{p}}_n)$ are the masses, positions, and momenta of the *photoactive quantum DOF* (i.e., the chromophore), respectively; $\{M_1,.. .,M_N\}$, $\mathbf{R} = (\mathbf{R}_1,.. .,\mathbf{R}_n)$, and $\mathbf{P} = (\mathbf{P}_1,.. .,\mathbf{P}_N)$ are the masses, positions, and momenta of the *photoinactive classical DOF* (i.e., the bath), respectively; $V(\hat{\mathbf{r}}, \mathbf{R})$ is the field-free potential energy, $\hat{H}$ is the field-free Hamiltonian, and $W(\hat{\mathbf{r}}, t)$ is the field-matter interaction term. The latter is assumed to be explicitly given by

$$W(\hat{\mathbf{r}}, t) = -\boldsymbol{\mu}(\hat{\mathbf{r}}) \cdot \mathbf{E}(t) \cos(\omega t - \phi) \quad (2)$$

where $\mathbf{E}(t)$, ω, and ϕ are the envelope, leading frequency, and phase of the driving field, respectively, and $\boldsymbol{\mu}(\hat{\mathbf{r}})$ is the chromophore's dipole moment operator.

Due to the mass separation between the photoactive (light) and photoinactive (heavy) DOF, it is convenient to consider the MQCL equation within a representation based on a basis that consists of the field-free adiabatic states, which are defined by

$$\hat{H}_{\mathrm{ad}}|\alpha(\mathbf{R})\rangle = E_\alpha(\mathbf{R})|\alpha(\mathbf{R})\rangle \quad (3)$$

Here, $\{|\alpha(\mathbf{R})\rangle\}$ and $\{E_\alpha(\mathbf{R})\}$ are the eigenstates and eigenvalues, respectively, of the explicitly $\mathbf{R}$-dependent adiabatic field-free Hamiltonian:

$$\hat{H}_{\mathrm{ad}}(\mathbf{R}) = \sum_{j=1}^{n} \frac{\hat{\mathbf{p}}_j^{\,2}}{2m_j} + V(\hat{\mathbf{r}}, \mathbf{R}) \quad (4)$$

In the next step, we consider the density operator of the overall system $\hat{\rho}(t)$. We first present it in terms of the partial Wigner transform with respect to the bath DOF:

$$\hat{\rho}_W(\mathbf{R}, \mathbf{P}; t) = \left(\frac{1}{2\pi\hbar}\right)^N \int \mathrm{d}\mathbf{Z}\, e^{i\mathbf{P}\cdot\Delta/\hbar} \langle \mathbf{R} - \Delta/2|\hat{\rho}(t)|\mathbf{R} + \Delta/2\rangle \quad (5)$$

The matrix elements of $\hat{\rho}_W(\mathbf{R}, \mathbf{P}; t)$, which is an operator in the chromophore's Hilbert space, in the adiabatic representation, are given by

$$\rho_W^{\alpha\alpha'}(\mathbf{R}, \mathbf{P}; t) = \langle \alpha(\mathbf{R})|\hat{\rho}_W(\mathbf{R}, \mathbf{P}; t)|\alpha'(\mathbf{R})\rangle \quad (6)$$

The MQCL equation of motion for $\rho_W^{\alpha\alpha'}(\mathbf{R}, \mathbf{P}; t)$ can then be shown to be given by[17,20−25]

$$\frac{\partial}{\partial t}\rho_W^{\alpha\alpha'}(\mathbf{R}, \mathbf{P}; t) = -i\omega_{\alpha\alpha'}(\mathbf{R})\, \rho_W^{\alpha\alpha'}(\mathbf{R}, \mathbf{P}; t)$$

$$- \mathbf{U}\cdot\vec{\nabla}_{\mathbf{R}}\rho_W^{\alpha\alpha'}(\mathbf{R}, \mathbf{P}; t) - \frac{\mathbf{F}^{\alpha\alpha}(\mathbf{R}) + \mathbf{F}^{\alpha'\alpha'}(\mathbf{R})}{2}\cdot\vec{\nabla}_{\mathbf{P}}\rho_W^{\alpha\alpha'}(\mathbf{R}, \mathbf{P}; t)$$

$$- \frac{i}{\hbar}\sum_\beta \left[W^{\alpha\beta}(\mathbf{R}; t)\, \rho_W^{\beta\alpha'}(\mathbf{R}, \mathbf{P}; t) - W^{\beta\alpha'}(\mathbf{R}; t)\, \rho_W^{\alpha\beta}(\mathbf{R}, \mathbf{P}; t)\right]$$

$$- \sum_{\beta\neq\alpha'} \mathbf{d}^*_{\alpha'\beta}\cdot\mathbf{U}\left[1 + \frac{1}{2}\mathbf{S}^*_{\alpha'\beta}(\mathbf{R})\cdot\vec{\nabla}_{\mathbf{P}}\right]\rho_W^{\alpha\beta}(\mathbf{R}, \mathbf{P}; t)$$

$$- \sum_{\beta\neq\alpha} \mathbf{d}_{\alpha\beta}\cdot\mathbf{U}\left[1 + \frac{1}{2}\mathbf{S}_{\alpha\beta}(\mathbf{R})\cdot\vec{\nabla}_{\mathbf{P}}\right]\rho_W^{\beta\alpha'}(\mathbf{R}, \mathbf{P}; t) \quad (7)$$

Here, $\mathbf{U} = \dot{\mathbf{R}}$, $\mathbf{F}^{\alpha\alpha}(\mathbf{R}) = -\vec{\nabla}_{\mathbf{R}}E_\alpha(\mathbf{R})$, $\mathbf{d}_{\alpha\beta}(\mathbf{R}) = -\mathbf{d}^*_{\beta\alpha}(\mathbf{R}) = \langle\alpha(\mathbf{R})|\vec{\nabla}_{\mathbf{R}}|\beta(\mathbf{R})\rangle$, $\omega_{\alpha\alpha'}(\mathbf{R}) = [E_\alpha(\mathbf{R}) - E_{\alpha'}(\mathbf{R})]/\hbar$, $\mathbf{S}_{\alpha\beta} = \hbar\omega_{\alpha\beta}(\mathbf{R})\mathbf{d}_{\alpha\beta}(\mathbf{R})/\mathbf{d}_{\alpha\beta}(\mathbf{R})\cdot\mathbf{U}$ and

$$W^{\alpha\beta}(\mathbf{R}; t) = -\boldsymbol{\mu}^{\alpha\beta}(\mathbf{R})\cdot\mathbf{E}(t)\cos(\omega t - \phi) \quad (8)$$

The first three terms on the RHS of eq 7 couple the phase space density $\rho_W^{\alpha\alpha'}(\mathbf{R}, \mathbf{P}; t)$ to itself and therefore correspond to *adiabatic* dynamics. The remaining terms couple $\rho_W^{\alpha\alpha'}(\mathbf{R}, \mathbf{P}; t)$ to either $\rho_W^{\alpha\beta}(\mathbf{R}, \mathbf{P}; t)$ (where $\beta \neq \alpha'$) or $\rho_W^{\beta\alpha'}(\mathbf{R}, \mathbf{P}; t)$ (where $\beta \neq \alpha$) terms and therefore correspond to *nonadiabatic* dynamics. The nonadiabatic terms can be further classified as radiative (i.e., terms involving $W^{\alpha\beta}(\mathbf{R}; t)$) or nonradiative (i.e., terms involving $\mathbf{d}_{\alpha\beta}(\mathbf{R})$), depending on whether or not they are triggered by field-matter interactions. The nonradiative nonadiabatic coupling terms are responsible for population relaxation processes which typically occur on time scales longer than those of the dynamics described by the adiabatic terms. In the previous study,[14] we neglected these nonadiabatic terms, thereby restricting ourselves to time scales that are shorter than the time scale required for them to affect the spectra. In the present study, we will take into account the effects of these nonradiative nonadiabatic terms as explained in the next section.

III. THIRD-ORDER OPTICAL RESPONSE IN THE PRESENCE OF NONADIABATIC TRANSITIONS

In this section, we will introduce a scheme for calculating the third-order ORFs in the case of a system whose dynamics is described by eq 7. For the sake of simplicity and concreteness, we will do so in the context of a two-state system. The two states will be denoted by $|0(\mathbf{R})\rangle$ and $|1(\mathbf{R})\rangle$, corresponding to the ground and excited field-free adiabatic states, respectively. The field-matter interaction term can then be put in the following form:

$$\hat{W}(t) = -\hat{\mu}E(t)\cos(\omega t - \varphi) \quad (9)$$

where

$$\hat{\mu} = \mu^{10}(\mathbf{R})\left[|0(\mathbf{R})\rangle\langle 1(\mathbf{R})| + |1(\mathbf{R})|\rangle\langle 0(\mathbf{R})|\right] \quad (10)$$

It should be noted that a two-state system involves only one transition dipole moment so that $E(t)$ corresponds to the component of the driving field which is parallel to it (assuming that the time scale for molecular rotation is longer than the time it takes to measure the optical response). It should also be noted that the adiabatic wave functions can always be chosen to be real, so that one can assume, without loss of generality, that $\mu^{10}(\mathbf{R}) = \mu^{01}(\mathbf{R})$.

In the next step, we consider the third-order quantum mechanical ORF given by[1]

$$S^{(3)}(t_3, t_2, t_1) = \left(\frac{i}{\hbar}\right)^3 Tr\left\{\hat{\mu}\mathbf{G}(t_3)\,\boldsymbol{\mu}\mathbf{G}(t_2)\,\boldsymbol{\mu}\mathbf{G}(t_1)\boldsymbol{\mu}\hat{\rho}_{\mathrm{eq}}\right\} \quad (11)$$

Here, $\hat{\rho}_{\mathrm{eq}} = \exp[-\beta\hat{H}]/Tr(\exp[-\beta\hat{H}])$, $\mathbf{G}(t)$ is the field-free Liouville-space retarded Green superoperator along a time interval of length t, $\boldsymbol{\mu}\hat{\rho} = [\hat{\mu}, \hat{\rho}]$, and $\hat{\mu}$ is as in eq 10. Rewriting eq 11 in terms of the partial Wigner representation, we obtain

$$S^{(3)}(t_3, t_2, t_1) \approx$$

$$\left(\frac{i}{\hbar}\right)^3 \int \mathrm{d}\mathbf{Z}_0\, Tr'\left\{\hat{\mu}\mathbf{G}_W(t_3)\,\boldsymbol{\mu}\mathbf{G}_W(t_2)\,\boldsymbol{\mu}\mathbf{G}_W(t_1)\,\boldsymbol{\mu}\hat{\rho}_W^{\mathrm{eq}}(\mathbf{Z}_0)\right\} \quad (12)$$

where $\mathbf{Z} = \{\mathbf{R}, \mathbf{P}\}$ and Tr' denotes a trace over the chromophore DOF. The operators $\hat{\mu}$ and $\hat{\rho}_W(\mathbf{Z})$ can be represented as

2×2 matrices in the adiabatic basis:

$$\hat{\mu} \doteq \begin{pmatrix} 0 & \mu^{10}(\mathbf{Z}) \\ \mu^{10}(\mathbf{Z}) & 0 \end{pmatrix}; \quad \hat{\rho}_W(\mathbf{Z}) \doteq \begin{pmatrix} \rho_W^{00}(\mathbf{Z}) & \rho_W^{01}(\mathbf{Z}) \\ \rho_W^{10}(\mathbf{Z}) & \rho_W^{11}(\mathbf{Z}) \end{pmatrix} \quad (13)$$

We will proceed by approximating the exact quantum-mechanical field-free dynamics, represented by $\mathbf{G}_W(t)$ in eq 12, by MQCL dynamics. It should also be noted that the field-matter interactions, represented by $\boldsymbol{\mu}$ in eq 12, are impulsive. Thus, the effect of acting with the dipole moment superoperator, $\boldsymbol{\mu} \equiv [\hat{\mu}, \cdot\,]$, is to reshuffle the populations and coherences without affecting $\mathbf{Z}$:

$$\boldsymbol{\mu} \begin{pmatrix} \rho_{\mathrm{eq},W}^{00}(\mathbf{Z}) & \rho_{\mathrm{eq},W}^{01}(\mathbf{Z}) \\ \rho_{\mathrm{eq},W}^{10}(\mathbf{Z}) & \rho_{\mathrm{eq},W}^{11}(\mathbf{Z}) \end{pmatrix}$$

$$= \mu^{10}(\mathbf{Z}) \begin{pmatrix} \rho_W^{10}(\mathbf{Z}) - \rho_W^{01}(\mathbf{Z}) & \rho_W^{11}(\mathbf{Z}) - \rho_W^{00}(\mathbf{Z}) \\ \rho_W^{00}(\mathbf{Z}) - \rho_W^{11}(\mathbf{Z}) & \rho_W^{01}(\mathbf{Z}) - \rho_W^{10}(\mathbf{Z}) \end{pmatrix} \quad (14)$$

In practice, one can describe the dynamics of the phase space densities $\rho_W^{00}(\mathbf{Z})$, $\rho_W^{01}(\mathbf{Z})$, $\rho_W^{10}(\mathbf{Z})$, and $\rho_W^{11}(\mathbf{Z})$ in terms of an ensemble of "nonadiabatic trajectories". The state of the system at each instant in time along such a trajectory is defined by the time dependence of three quantities, $\{\mathbf{Z}_t\{\alpha\beta\}_t, F_t\}$, which are defined as follows:

(1) $\mathbf{Z} = \{\mathbf{R}, \mathbf{P}\}$ corresponds to the set of bath coordinates and momenta.
(2) $\{\alpha\beta\}$ denotes the PES that governs the bath dynamics: $V_{\alpha\beta}(\mathbf{R}) \equiv (E_\alpha(\mathbf{R}) + E_\beta(\mathbf{R}))/2$.
(3) F is a cumulative weighting factor that accounts for phase accumulation when $\alpha \neq \beta$ by $\exp[\pm i \int_0^t \mathrm{d}\tau\, \omega_{\alpha\beta}(\mathbf{Z}_\tau)]$, as well as for interaction with the field by $\pm\mu_{10}(\mathbf{Z})$ (see below).

Thus, the effect of acting with the dipole superoperator is to split the nonadiabatic trajectory in the following manner (see eq 14):

$$\{\mathbf{Z}, 00, F\} \rightarrow \begin{cases} \{\mathbf{Z}, 01, -\mu^{10}(\mathbf{Z})F\} \\ \{\mathbf{Z}, 10, \mu^{10}(\mathbf{Z})F\} \end{cases};$$

$$\{\mathbf{Z}, 11, F\} \rightarrow \begin{cases} \{\mathbf{Z}, 01, \mu^{10}(\mathbf{Z})F\} \\ \{\mathbf{Z}, 10, -\mu^{10}(\mathbf{Z})F\} \end{cases}$$

$$\{\mathbf{Z}, 01, F\} \rightarrow \begin{cases} \{\mathbf{Z}, 00, -\mu^{10}(\mathbf{Z})F\} \\ \{\mathbf{Z}, 11, \mu^{10}(\mathbf{Z})F\} \end{cases};$$

$$\{\mathbf{Z}, 10, F\} \rightarrow \begin{cases} \{\mathbf{Z}, 00, \mu^{10}(\mathbf{Z})F\} \\ \{\mathbf{Z}, 11, -\mu^{10}(\mathbf{Z})F\} \end{cases} \quad (15)$$

It should be noted that each trajectory splits into two and that the relative weights of the emergent two trajectories are determined by the instantaneous value of the transition dipole moment at the time of the field-matter interaction, $\mu^{10}(\mathbf{Z})$, thereby accounting for non-Condon effects.

By considering the successive action of each operator from right to left in eq 11, we may then obtain a mixed quantum-classical prescription for calculating the third-order ORF. The first step involves the interaction of the chromophore with a single impulsive pulse at time $t = 0$. We assume that the energy gap between the ground and excited states is significantly larger than $k_B T$. Thus, the initial equilibrium state prior to the first interaction with the field corresponds to having the chromophore in its ground state and the photoinactive DOF in the corresponding thermal equilibrium state:

$$\hat{\rho} w(\mathbf{Z}_0; 0_-) \doteq \begin{pmatrix} \rho_{\mathrm{eq},W}^{00}(\mathbf{Z}_0) & 0 \\ 0 & 0 \end{pmatrix} \quad (16)$$

Here, $\rho_{\mathrm{eq},W}^{00}(\mathbf{Z}_0)$ is the Wigner transform of the ground state equilibrium density operator, $\hat{\rho}_{\mathrm{eq}}^{00} = \exp[-\beta\hat{H}_0]/Tr(\exp[-\beta\hat{H}_0])$, where $\hat{H}_0 = \sum_{J=1}^{N}(\hat{\mathbf{P}}_J^2/2M_J) + E_0(\hat{\mathbf{R}})$. This implies that $\alpha_0\beta_0 = 00$ and $F_0 = 1$ for all trajectories and $\mathbf{Z}_0$ is sampled based on $\rho_{\mathrm{eq},W}^{00}(\mathbf{Z}_0)$. In practice, one can usually assume that $\rho_{\mathrm{eq},W}^{00}(\mathbf{Z}_0)$ can be well approximated by its classical limit:

$$\rho_{\mathrm{eq},W}^{00}(\mathbf{Z}_0) \approx \exp[-\beta H_0(\mathbf{Z}_0)] / \int \mathrm{d}Z_0 \exp[-\beta H_0(\mathbf{Z}_0)] \quad (17)$$

Now, consider a single nonadiabatic trajectory that starts at a particular $\mathbf{Z}_0$, such that the initial state is given by $\{\mathbf{Z}_0, 00, 1\}$. According to eq 15, the impact of the first interaction with the field is to change $\alpha\beta = 00$ into either 01 or 10 in an impulsive manner:

$$\{\mathbf{Z}_0, 00, 1\} \rightarrow \begin{cases} \{\mathbf{Z}_0, 01, -\mu^{10}(\mathbf{Z}_0)\} \\ \{\mathbf{Z}_0, 10, \mu^{10}(\mathbf{Z}_0)\} \end{cases} \quad (18)$$

It should also be noted that the two emergent trajectories are weighted by the values of the transition dipole moment at the moment of interaction, namely, $\mu^{10}(\mathbf{Z}_0)$ and $-\mu^{01}(\mathbf{Z}_0)$, respectively, so that F should be modified from 1 to either $\mu^{10}(\mathbf{Z}_0)$ or $-\mu^{01}(\mathbf{Z}_0)$, depending on whether $\alpha\beta$ changed into either 10 or 01, respectively.

The field-free dynamics during the time interval $(0, t_1)$ between the first and second field-matter interactions is described by eq 7 with $W^{\alpha\beta}(\mathbf{R}, t) = 0$. It should be noted that the dynamical range of t_1 is dictated by the dephasing time which is typically significantly shorter than the population relaxation time. We will therefore assume that t_1 is short enough so that no nonadiabatic transitions occur during this time interval. To this end, we will set $\mathbf{d}_{\alpha\beta} = 0$ during the time interval $(0, t_1)$. Thus, the phase space densities $\rho_W^{01}(\mathbf{Z})$ and $\rho_W^{10}(\mathbf{Z})$ are to be propagated classically and independently from one another on the *average* PES, $V_{01}(\mathbf{R}) = [E_0(\mathbf{R}) + E_1(\mathbf{R})]/2$, during the time interval $(0, t_1)$. In practice, this can be achieved by sampling initial conditions at $t = 0$ from $\rho_{\mathrm{eq},W}^{00}(\mathbf{Z})$ followed by simulating their nonequilibrium dynamics on the average PES $V_{10}(\mathbf{R})$ for a period of time t_1 while accumulating phase factors of the form $\exp[-i\int_0^t \mathrm{d}\tau\, \omega_{10}(\mathbf{R}_\tau)]$ or $\exp[i\int_0^t \mathrm{d}\tau\, \omega_{10}(\mathbf{R}_\tau)]$, respectively:

$$\begin{cases} \{\mathbf{Z}_0, 01, -\mu^{10}(\mathbf{Z}_0)\} \\ \{\mathbf{Z}_0, 10, \mu^{10}(\mathbf{Z}_0)\} \end{cases} \rightarrow$$

$$\begin{cases} \left\{\mathbf{Z}_{t_1}^{10}, 01, -\mu^{10}(\mathbf{Z}_0) \exp\left[i\int_0^{t_1} \mathrm{d}\tau \omega_{10}(\mathbf{Z}_\tau^{10})\right]\right\} \\ \left\{\mathbf{Z}_{t1}^{10}, 10, \mu^{10}(\mathbf{Z}_0) \exp\left[-i\int_0^{t_1} \mathrm{d}\tau \omega_{10}(\mathbf{Z}_\tau^{10})\right]\right\} \end{cases} \quad (19)$$

Here, $\mathbf{Z}_\tau^{10}$ is the bath state after being propagated, starting at $\mathbf{Z}_0$, for a period of time τ on the average PES. It should be noted that, within this description, dephasing arises from averaging the phase factor $\exp[i\int_0^t \mathrm{d}\tau\, \omega_{10}(\mathbf{R}_\tau)]$ over the initial conditions. More specifically, the fact that different initial conditions lead to different trajectories of the transition frequency $\omega_{10}(\mathbf{R}_\tau)$ gives rise to a distribution of $\int_0^t \mathrm{d}\tau\, \omega_{10}(\mathbf{R}_\tau)$ which becomes broader with time and thereby diminishes the signal due to destructive interference.

dx.doi.org/10.1021/jp1061495 |J. Phys. Chem. B 2011, 115, 5191–5200

The second field-matter interaction at time t_1 splits the trajectories yet again as follows (see eq 15):

$$\left\{\mathbf{Z}_{t_1}^{10}, 01, -\mu^{10}(\mathbf{Z}_0)\, e^{i\int_0^{t_1} d\tau\omega_{10}(\mathbf{Z}_\tau^{10})}\right\} \rightarrow$$

$$\left\{\begin{array}{l}\left\{\mathbf{Z}_{t_1}^{10}, 00, \overbrace{\mu^{10}(\mathbf{Z}_0)\,\mu^{10}(\mathbf{Z}_{t_1})\, e^{i\int_0^{t_1} d\tau\omega_{10}(\mathbf{Z}_\tau^{10})}}^{F_3}\right\} \\ \left\{\mathbf{Z}_{t_1}^{10}, 11, -\overbrace{\mu^{10}(\mathbf{Z}_0)\,\mu^{10}(\mathbf{Z})\, e^{i\int_0^{t_1} d\tau\omega_{10}(\mathbf{Z}_\tau^{10})}}^{F_2}\right\}\end{array}\right.$$

$$\left\{\mathbf{Z}_{t_1}^{10}, 10, \mu^{10}(\mathbf{Z}_0)\, e^{-i\int_0^{t_1} d\tau\omega_{10}(\mathbf{Z}_\tau^{10})}\right\} \rightarrow$$

$$\left\{\begin{array}{l}\left\{\mathbf{Z}_{t_1}^{10}, 00, \overbrace{\mu^{10}(\mathbf{Z}_0)\,\mu^{10}(\mathbf{Z}_{t_1})\, e^{-i\int_0^{t_1} d\tau\omega_{10}(\mathbf{Z}_\tau^{10})}}^{F_4}\right\} \\ \left\{\mathbf{Z}_{t_1}^{10}, 11, -\overbrace{\mu^{10}(\mathbf{Z}_0)\,\mu^{10}(\mathbf{Z}_{t_1})\, e^{-i\int_0^{t_1} d\tau\omega_{10}(\mathbf{Z}_\tau^{10})}}^{F_1}\right\}\end{array}\right. \quad (20)$$

Following the second field-matter interaction, the system undergoes field-free evolution during the time interval $(t_1, t_1 + t_2)$. As long as $\alpha\beta$ remains equal to either 00 (ground state PES) or 11 (excited state PES), there is no phase accumulation and therefore no dephasing. As a result, t_2 can be significantly longer than t_1 and the only mechanism that can diminish the signal as a function of t_2 corresponds to nonadiabatic transitions.

In the case of a two-state system, the MQCL equation, eq 7, does not allow for a direct nonadiabatic transition from state 11 into state 00. Instead, the system must first pass through the 10 or 01 states before reaching the 00 state. However, the contributions from trajectories that remain in either the 10 or 01 states would diminish rapidly due to dephasing. Thus, in practice, one can assume that only trajectories that undergo such rapid transitions from the 10/01 states into the 00 state contribute to the signal. As a result, population loss from the 11 state can be assumed to imply population gain in the 00 state. In other words, we can treat the nonadiabatic transitions between 11 and 00 as if they occurred in a direct manner. Moreover, we assume that trajectories which hopped from 10 and 01 into 00 at time t_1 will continue to evolve on the 00 PES during the time interval $(t_1, t_1 + t_2)$:

$$\begin{array}{l}\left\{\mathbf{Z}_{t_1}^{10}, 00, F_3\right\} \rightarrow \left\{\mathbf{Z}_{t_1+t_2}^{10,00}, 00, F_3\right\} \\ \left\{\mathbf{Z}_{t_1}^{10}, 00, F_4\right\} \rightarrow \left\{\mathbf{Z}_{t_1+t_2}^{10,00}, 00, F_4\right\}\end{array} \quad (21)$$

where $\mathbf{Z}_{t_1+t_2}^{10,00}$ are trajectories that took place on the 10 PES during the time interval $(0, t_1)$ and the 00 PES during the time interval $(t_1, t_1 + t_2)$. However, those trajectories that hopped from 10 and 01 into 11 at time t_1 will eventually undergo nonadiabatic transitions during the time interval $(t_1, t_1 + t_2)$, as follows:

$$\left\{\mathbf{Z}_{t_1}^{10}, 11, -F_1\right\} \rightarrow \left\{\begin{array}{l}\left\{\mathbf{Z}_{t_1+t_2}^{10,(11,00)}, 00, -F_1\right\} \\ \left\{\mathbf{Z}_{t_1+t_2}^{10,(11,11)}, 11, -F_1\right\}\end{array}\right.;$$

$$\left\{\mathbf{Z}_{t_1}^{10}, 11, -F_2\right\} \rightarrow \left\{\begin{array}{l}\left\{\mathbf{Z}_{t_1+t_2}^{10,(11,00)}, 00, -F_2\right\} \\ \left\{\mathbf{Z}_{t_1+t_2}^{10,(11,11)}, 11, -F_2\right\}\end{array}\right. \quad (22)$$

Here, $\mathbf{Z}_{t_1+t_2}^{10,(11,00)}$ and $\mathbf{Z}_{t_1+t_2}^{10,(11,11)}$ correspond to trajectories that were propagated on the 10 PES during the time interval $(0, t_1)$, hopped to the 11 PES at time t_1, and then either hopped or not to the 00 PES by the time $t_1 + t_2$, depending on whether or not a nonadiabatic transition took place during the time interval $(t_1, t_1 + t_2)$.

The third field-matter interaction at time $t_1 + t_2$ splits the trajectories as follows:

$$\left\{\mathbf{Z}_{t_1+t_2}^{10,00}, 00, F_3\right\} \rightarrow \left\{\begin{array}{l}\left\{\mathbf{Z}_{t_1+t_2}^{10,00}, 01, -\mu^{10}(\mathbf{Z}_{t_1+t_2}^{10,00})F_3\right\} \\ \left\{\mathbf{Z}_{t_1+t_2}^{10,00}, 10, \mu^{10}(\mathbf{Z}_{t_1+t_2}^{10,00})F_3\right\}\end{array}\right.$$

$$\left\{\mathbf{Z}_{t_1+t_2}^{10,00}, 00, F_4\right\} \rightarrow \left\{\begin{array}{l}\left\{\mathbf{Z}_{t_1+t_2}^{10,00}, 01, -\mu^{10}(\mathbf{Z}_{t_1+t_2}^{10,00})F_4\right\} \\ \left\{\mathbf{Z}_{t_1+t_2}^{10,00}, 10, \mu^{10}(\mathbf{Z}_{t_1+t_2}^{10,00})F_4\right\}\end{array}\right. \quad (23)$$

$$\left\{\mathbf{Z}_{t_1+t_2}^{10,(11,00)}, 00, -F_1\right\} \rightarrow \left\{\begin{array}{l}\left\{\mathbf{Z}_{t_1+t_2}^{10,(11,00)}, 01, \mu^{10}(\mathbf{Z}_{t_1+t_2}^{10,(11,00)})F_1\right\} \\ \left\{\mathbf{Z}_{t_1+t_2}^{10,(11,00)}, 10, -\mu^{10}(\mathbf{Z}_{t_1+t_2}^{10,(11,00)})F_1\right\}\end{array}\right.$$

$$\left\{\mathbf{Z}_{t_1+t_2}^{10,(11,11)}, 11, -F_1\right\} \rightarrow \left\{\begin{array}{l}\left\{\mathbf{Z}_{t_1+t_2}^{10,(11,11)}, 01, -\mu^{10}(\mathbf{Z}_{t_1+t_2}^{10,(11,11)})F_1\right\} \\ \left\{\mathbf{Z}_{t_1+t_2}^{10,(11,11)}, 10, \mu^{10}(\mathbf{Z}_{t_1+t_2}^{10,(11,11)})F_1\right\}\end{array}\right. \quad (24)$$

$$\left\{\mathbf{Z}_{t_1+t_2}^{10,(11,00)}, 00, -F_2\right\} \rightarrow \left\{\begin{array}{l}\left\{\mathbf{Z}_{t_1+t_2}^{10,(11,00)}, 01, \mu^{10}(\mathbf{Z}_{t_1+t_2}^{10,(11,00)})F_2\right\} \\ \left\{\mathbf{Z}_{t_1+t_2}^{10,(11,00)}, 10, -\mu^{10}(\mathbf{Z}_{t_1+t_2}^{10,(11,00)})F_2\right\}\end{array}\right.$$

$$\left\{\mathbf{Z}_{t_1+t_2}^{10,(11,11)}, 11, -F_2\right\} \rightarrow \left\{\begin{array}{l}\left\{\mathbf{Z}_{t_1+t_2}^{10,(11,11)}, 01, -\mu^{10}(\mathbf{Z}_{t_1+t_2}^{10,(11,11)})F_2\right\} \\ \left\{\mathbf{Z}_{t_1+t_2}^{10,(11,11)}, 10, \mu^{10}(\mathbf{Z}_{t_1+t_2}^{10,(11,11)})F_2\right\}\end{array}\right. \quad (25)$$

Following this, the system undergoes field-free evolution during the time interval $(t_1 + t_2, t_1 + t_2 + t_3)$. It should be noted that $\alpha \neq \beta$ at $t > t_1 + t_2$, so that phase will be accumulated during the time interval $(t_1 + t_2, t_1 + t_2 + t_3)$, thereby leading to dephasing. Thus, as for t_1, we will assume that t_3 is short enough such that no nonadiabatic transitions occur during this time interval:

$$\left\{\mathbf{Z}_{t_1+t_2}^{10,00}, 01, -\mu^{10}(\mathbf{Z}_{t_1+t_2}^{10,00})F_3\right\}$$

$$\rightarrow \left\{\mathbf{Z}_{t_1+t_2+t_3}^{10,00,10}, 01, -\mu^{10}(\mathbf{Z}_{t_1+t_2}^{10,00})F_3\, e^{-i\int_{t_1+t_2}^{t_1+t_2+t_3} d\tau\omega_{10}(\mathbf{Z}_{t_1+t_2+\tau}^{10,00,10})}\right\}$$

$$\left\{\mathbf{Z}_{t_1+t_2}^{10,00}, 10, \mu^{10}(\mathbf{Z}_{t_1+t_2}^{10,00})F_3\right\}$$

$$\rightarrow \left\{\mathbf{Z}_{t_1+t_2+t_3}^{10,00,10}, 10, \mu^{10}(\mathbf{Z}_{t_1+t_2}^{10,00})F_3\, e^{-i\int_{t_1+t_2}^{t_1+t_2+t_3} d\tau\omega_{10}(\mathbf{Z}_{t_1+t_2+\tau}^{10,00,10})}\right\}$$

$$\left\{\mathbf{Z}_{t_1+t_2}^{10,00}, 01, -\mu^{10}(\mathbf{Z}_{t_1+t_2}^{10,00})F_4\right\}$$

$$\rightarrow \left\{\mathbf{Z}_{t_1+t_2+t_3}^{10,00,10}, 01, -\mu^{10}(\mathbf{Z}_{t_1+t_2}^{10,00})F_4\, e^{-i\int_{t_1+t_2}^{t_1+t_2+t_3} d\tau\omega_{10}(\mathbf{Z}_{t_1+t_2+\tau}^{10,00,10})}\right\}$$

$$\left\{\mathbf{Z}_{t_1+t_2}^{10,00}, 10, \mu^{10}(\mathbf{Z}_{t_1+t_2}^{10,00})F_4\right\}$$

$$\rightarrow \left\{\mathbf{Z}_{t_1+t_2+t_3}^{10,00,10}, 10, \mu^{10}(\mathbf{Z}_{t_1+t_2}^{10,00})F_4 e^{-i\int_{t_1+t_2}^{t_1+t_2+t_3} d\tau\omega_{10}(\mathbf{Z}_{t_1+t_2+\tau}^{10,00,10})}\right\} \quad (26)$$

dx.doi.org/10.1021/jp1061495 |J. Phys. Chem. B 2011, 115, 5191–5200

$$
\begin{aligned}
\left\{\mathbf{Z}_{t_1+t_2}^{10,(11,00)}, 01, \mu^{10}(\mathbf{Z}_{t_1+t_2}^{10,(11,00)})F_1\right\} &\rightarrow \left\{\mathbf{Z}_{t_1+t_2+t_3}^{10,(11,00)}, 01, \mu^{10}(\mathbf{Z}_{t_1+t_2}^{10,(11,00)})F_1\, e^{i\int_{t_1+t_2}^{t_1+t_2+t_3} d\tau\omega_{10}(\mathbf{Z}_{t_1+t_2+\tau}^{10,(11,00),10})}\right\}\\
\left\{\mathbf{Z}_{t_1+t_2}^{10,(11,00)}, 10, -\mu^{10}(\mathbf{Z}_{t_1+t_2}^{10,(11,00)})F_1\right\} &\rightarrow \left\{\mathbf{Z}_{t_1+t_2+t_3}^{10,(11,00),10}, 10, -\mu^{10}(\mathbf{Z}_{t_1+t_2}^{10,(11,00)})F_1\, e^{-i\int_{t_1+t_2}^{t_1+t_2+t_3} d\tau\omega_{10}(\mathbf{Z}_{t_1+t_2+\tau}^{10,(11,00),10})}\right\}\\
\left\{\mathbf{Z}_{t_1+t_2}^{10,(11,11)}, 01, -\mu^{10}(\mathbf{Z}_{t_1+t_2}^{10,(11,11)})F_1\right\} &\rightarrow \left\{\mathbf{Z}_{t_1+t_2+t_3}^{10,(11,11),10}, 01, -\mu^{10}(\mathbf{Z}_{t_1+t_2}^{10,(11,11)})F_1\, e^{i\int_{t_1+t_2}^{t_1+t_2+t_3} d\tau\omega_{10}(\mathbf{Z}_{t_1+t_2+\tau}^{10,(11,11),10})}\right\}\\
\left\{\mathbf{Z}_{t_1+t_2}^{10,(11,11)}, 10, \mu^{10}(\mathbf{Z}_{t_1+t_2}^{10,(11,11)})F_1\right\} &\rightarrow \left\{\mathbf{Z}_{t_1+t_2+t_3}^{10,(11,11),10}, 10, \mu^{10}(\mathbf{Z}_{t_1+t_2}^{10,(11,11)})F_1\, e^{-i\int_{t_1+t_2}^{t_1+t_2+t_3} d\tau\omega_{10}(\mathbf{Z}_{t_1+t_2+\tau}^{10,(11,11),10})}\right\}
\end{aligned}
\tag{27}
$$

$$
\begin{aligned}
\left\{\mathbf{Z}_{t_1+t_2}^{10,(11,00)}, 01, \mu^{10}(\mathbf{Z}_{t_1+t_2}^{10,(11,00)})F_2\right\} &\rightarrow \left\{\mathbf{Z}_{t_1+t_2+t_3}^{10,(11,00),10}, 01, \mu^{10}(\mathbf{Z}_{t_1+t_2}^{10,(11,00)})F_2\, e^{i\int_{t_1+t_2}^{t_1+t_2+t_3} d\tau\omega_{10}(\mathbf{Z}_{t_1+t_2+\tau}^{10,(11,00),10})}\right\}\\
\left\{\mathbf{Z}_{t_1+t_2}^{10,(11,00)}, 10, -\mu^{10}(\mathbf{Z}_{t_1+t_2}^{10,(11,00)})F_2\right\} &\rightarrow \left\{\mathbf{Z}_{t_1+t_2+t_3}^{10,(11,00),10}, 10, -\mu^{10}(\mathbf{Z}_{t_1+t_2}^{10,(11,00)})F_2\, e^{-i\int_{t_1+t_2}^{t_1+t_2+t_3} d\tau\omega_{10}(\mathbf{Z}_{t_1+t_2+\tau}^{10,(11,00),10})}\right\}\\
\left\{\mathbf{Z}_{t_1+t_2}^{10,(11,11)}, 01, -\mu^{10}(\mathbf{Z}_{t_1+t_2}^{10,(11,11)})F_2\right\} &\rightarrow \left\{\mathbf{Z}_{t_1+t_2+t_3}^{10,(11,11),10}, 01, -\mu^{10}(\mathbf{Z}_{t_1+t_2}^{10,(11,11)})F_2\, e^{i\int_{t_1+t_2}^{t_1+t_2+t_3} d\tau\omega_{10}(\mathbf{Z}_{t_1+t_2+\tau}^{10,(11,11),10})}\right\}\\
\left\{\mathbf{Z}_{t_1+t_2}^{10,(11,11)}, 10, \mu^{10}(\mathbf{Z}_{t_1+t_2}^{10,(11,11)})F_2\right\} &\rightarrow \left\{\mathbf{Z}_{t_1+t_2+t_3}^{10,(11,11),10}, 10, \mu^{10}(\mathbf{Z}_{t_1+t_2}^{10,(11,11)})F_2\, e^{-i\int_{t_1+t_2}^{t_1+t_2+t_3} d\tau\omega_{10}(\mathbf{Z}_{t_1+t_2+\tau}^{10,(11,11),10})}\right\}
\end{aligned}
\tag{28}
$$

Finally, operating with the dipole moment operator from the left at time $t_1 + t_2 + t_3$ and tracing leads to the following mixed quantum-classical expression for the third-order ORF:

$$
\begin{aligned}
S^{(3)}(t_3,t_2,t_1) = \left(\tfrac{i}{\hbar}\right)^3 \int \mathbf{dZ}_0 \rho_{W,eq}^{00}(\mathbf{Z}_0) \times \\
\left\{
\begin{array}{l}
-\mu^{10}(\mathbf{Z}_0)\,\mu^{10}(\mathbf{Z}_{t_1})\,\mu^{10}\left(\mathbf{Z}_{t_1+t_2}^{10,00}\right)\mu^{10}\left(\mathbf{Z}_{t_1+t_2+t_3}^{10,00,10}\right) e^{i\int_0^{t_1} d\tau\omega_{10}\left(\mathbf{Z}_\tau^{10}\right)+i\int_{t_1+t_2}^{t_1+t_2+t_3} d\tau\omega_{10}\left(\mathbf{Z}_{t_1+t_2+\tau}^{10,00,10}\right)}\\
\mu^{10}(\mathbf{Z}_0)\,\mu^{10}(\mathbf{Z}_{t_1})\,\mu^{10}\left(\mathbf{Z}_{t_1+t_2}^{10,00}\right)\mu^{10}\left(\mathbf{Z}_{t_1+t_2+t_3}^{10,00,10}\right) e^{i\int_0^{t_1} d\tau\omega_{10}\left(\mathbf{Z}_\tau^{10}\right)-i\int_{t_1+t_2}^{t_1+t_2+t_3} d\tau\omega_{10}\left(\mathbf{Z}_{t_1+t_2+\tau}^{10,00,10}\right)}\\
-\mu^{10}(\mathbf{Z}_0)\,\mu^{10}(\mathbf{Z}_{t_1})\,\mu^{10}\left(\mathbf{Z}_{t_1+t_2}^{10,00}\right)\mu^{10}\left(\mathbf{Z}_{t_1+t_2+t_3}^{10,00,10}\right) e^{-i\int_0^{t_1} d\tau\omega_{10}\left(\mathbf{Z}_\tau^{10}\right)+i\int_{t_1+t_2}^{t_1+t_2+t_3} d\tau\omega_{10}\left(\mathbf{Z}_{t_1+t_2+\tau}^{10,00,10}\right)}\\
+\mu^{10}(\mathbf{Z}_0)\,\mu^{10}(\mathbf{Z}_{t_1})\,\mu^{10}\left(\mathbf{Z}_{t_1+t_2}^{10,00}\right)\mu^{10}\left(\mathbf{Z}_{t_1+t_2+t_3}^{10,00,10}\right) e^{-i\int_0^{t_1} d\tau\omega_{10}\left(\mathbf{Z}_\tau^{10}\right)-i\int_{t_1+t_2}^{t_1+t_2+t_3} d\tau\omega_{10}\left(\mathbf{Z}_{t_1+t_2+\tau}^{10,00,10}\right)}\\
+\mu^{10}(\mathbf{Z}_0)\,\mu^{10}(\mathbf{Z}_{t_1})\,\mu^{10}\left(\mathbf{Z}_{t_1+t_2}^{10,(11,00)}\right)\mu^{10}\left(\mathbf{Z}_{t_1+t_2+t_3}^{10,(11,00),10}\right) e^{-i\int_0^{t_1} d\tau\omega_{10}\left(\mathbf{Z}_\tau^{10}\right)+i\int_{t_1+t_2}^{t_1+t_2+t_3} d\tau\omega_{10}\left(\mathbf{Z}_{t_1+t_2+\tau}^{10,(11,00),10}\right)}\\
-\mu^{10}(\mathbf{Z}_0)\,\mu^{10}(\mathbf{Z}_{t_1})\,\mu^{10}\left(\mathbf{Z}_{t_1+t_2}^{10,(11,00)}\right)\mu^{10}\left(\mathbf{Z}_{t_1+t_2+t_3}^{10,(11,00),10}\right) e^{-i\int_0^{t_1} d\tau\omega_{10}\left(\mathbf{Z}_\tau^{10}\right)-i\int_{t_1+t_2}^{t_1+t_2+t_3} d\tau\omega_{10}\left(\mathbf{Z}_{t_1+t_2+\tau}^{10,(11,00),10}\right)}\\
-\mu^{10}(\mathbf{Z}_0)\,\mu^{10}(\mathbf{Z}_{t_1})\,\mu^{10}\left(\mathbf{Z}_{t_1+t_2}^{10,(11,11)}\right)\mu^{10}\left(\mathbf{Z}_{t_1+t_2+t_3}^{10,(11,11),10}\right) e^{-i\int_0^{t_1} d\tau\omega_{10}\left(\mathbf{Z}_\tau^{10}\right)+i\int_{t_1+t_2}^{t_1+t_2+t_3} d\tau\omega_{10}\left(\mathbf{Z}_{t_1+t_2+\tau}^{10,(11,11),10}\right)}\\
+\mu^{10}(\mathbf{Z}_0)\,\mu^{10}(\mathbf{Z}_{t_1})\,\mu^{10}\left(\mathbf{Z}_{t_1+t_2}^{10,(11,11)}\right)\mu^{10}\left(\mathbf{Z}_{t_1+t_2+t_3}^{10,(11,11),10}\right) e^{-i\int_0^{t_1} d\tau\omega_{10}\left(\mathbf{Z}_\tau^{10}\right)-i\int_{t_1+t_2}^{t_1+t_2+t_3} d\tau\omega_{10}\left(\mathbf{Z}_{t_1+t_2+\tau}^{10,(11,11),10}\right)}\\
+\mu^{10}(\mathbf{Z}_0)\,\mu^{10}(\mathbf{Z}_{t_1})\,\mu^{10}\left(\mathbf{Z}_{t_1+t_2}^{10,(11,00)}\right)\mu^{10}\left(\mathbf{Z}_{t_1+t_2+t_3}^{10,(11,00),10}\right) e^{i\int_0^{t_1} d\tau\omega_{10}\left(\mathbf{Z}_\tau^{10}\right)+i\int_{t_1+t_2}^{t_1+t_2+t_3} d\tau\omega_{10}\left(\mathbf{Z}_{t_1+t_2+\tau}^{10,(11,00),10}\right)}\\
-\mu^{10}(\mathbf{Z}_0)\,\mu^{10}(\mathbf{Z}_{t_1})\,\mu^{10}\left(\mathbf{Z}_{t_1+t_2}^{10,(11,00)}\right)\mu^{10}\left(\mathbf{Z}_{t_1+t_2+t_3}^{10,(11,00),10}\right) e^{i\int_0^{t_1} d\tau\omega_{10}\left(\mathbf{Z}_\tau^{10}\right)-i\int_{t_1+t_2}^{t_1+t_2+t_3} d\tau\omega_{10}\left(\mathbf{Z}_{t_1+t_2+\tau}^{10,(11,00),10}\right)}\\
-\mu^{10}(\mathbf{Z}_0)\,\mu^{10}(\mathbf{Z}_{t_1})\,\mu^{10}\left(\mathbf{Z}_{t_1+t_2}^{10,(11,11)}\right)\mu^{10}\left(\mathbf{Z}_{t_1+t_2+t_3}^{10,(11,11),10}\right) e^{i\int_0^{t_1} d\tau\omega_{10}\left(\mathbf{Z}_\tau^{10}\right)+i\int_{t_1+t_2}^{t_1+t_2+t_3} d\tau\omega_{10}\left(\mathbf{Z}_{t_1+t_2+\tau}^{10,(11,11),10}\right)}\\
+\mu^{10}(\mathbf{Z}_0)\,\mu^{10}(\mathbf{Z}_{t_1})\,\mu^{10}\left(\mathbf{Z}_{t_1+t_2}^{10,(11,11)}\right)\mu^{10}\left(\mathbf{Z}_{t_1+t_2+t_3}^{10,(11,11),10}\right) e^{i\int_0^{t_1} d\tau\omega_{10}\left(\mathbf{Z}_\tau^{10}\right)-i\int_{t_1+t_2}^{t_1+t_2+t_3} d\tau\omega_{10}\left(\mathbf{Z}_{t_1+t_2+\tau}^{10,(11,11),10}\right)}
\end{array}
\right\}
\end{aligned}
\tag{29}
$$

The third-order response signal field is given by[1]

$$
P^{(3)}(t) = \int_0^\infty dt_3 \int_0^\infty dt_2 \int_0^\infty dt_1 S^{(3)}(t_3,t_2,t_1)\, E(t-t_3)\, E(t-t_3-t_2)\, E(t-t_3-t_2-t_1)
\tag{30}
$$

We now restrict ourselves to the case of three consecutive nonoverlapping impulsive driving fields along wave vectors $\mathbf{k_a}$, $\mathbf{k_b}$, and $\mathbf{k_c}$, which are assumed to have the same leading frequency (pulse *a* is assumed to precede pulse *b* which in turn precedes pulse *c*). Within the rotating wave approximation (RWA), it can be shown that in this situation the two signal fields in the background-free directions $\mathbf{k_r} = -\mathbf{k_a} + \mathbf{k_b} + \mathbf{k_c}$ and $\mathbf{k_{nr}} = \mathbf{k_a} - \mathbf{k_b} + \mathbf{k_c}$, corresponding to the *rephasing* and *nonrephasing* signals, respectively, are

$$P^{(3)}_{\mathrm{nr}}(t_1,t_2,t_3) = \langle \mu^{10}(\mathbf{Z}_0)\,\mu^{10}(\mathbf{Z}_{t_1})\,\mu^{10}(\mathbf{Z}^{10,00}_{t_1+t_2})\,\mu^{10}(\mathbf{Z}^{10,00,10}_{t_1+t_2+t_3}) \times \mathrm{e}^{-i\int_0^{t_1}\mathrm{d}\tau\omega_{10}(\mathbf{Z}^{10}_\tau)-i\int_{t_1+t_2}^{t_1+t_2+t_3}\mathrm{d}\tau\omega_{10}(\mathbf{Z}^{10,00,10}_{t_1+t_2+\tau})}\rangle_{00} + \langle \mu^{10}(\mathbf{Z}_0)\,\mu^{10}(\mathbf{Z}_{t_1})\,\mu^{10}(\mathbf{Z}^{10,(11,11)}_{t_1+t_2})\,\mu^{10}(\mathbf{Z}^{10,(11,11),10}_{t_1+t_2+t_3}) \times \mathrm{e}^{-i\int_0^{t_1}\mathrm{d}\tau\omega_{10}(\mathbf{Z}^{10}_\tau)-i\int_{t_1+t_2}^{t_1+t_2+t_3}\mathrm{d}\tau\omega_{10}(\mathbf{Z}^{10,(11,11),10}_{t_1+t_2+\tau})}\rangle_{00} - \langle \mu^{10}(\mathbf{Z}_0)\,\mu^{10}(\mathbf{Z}_{t_1})\,\mu^{10}(\mathbf{Z}^{10,(11,00)}_{t_1+t_2})\,\mu^{10}(\mathbf{Z}^{10,(11,00),10}_{t_1+t_2+t_3}) \times \mathrm{e}^{-i\int_0^{t_1}\mathrm{d}\tau\omega_{10}(\mathbf{Z}^{10}_\tau)-i\int_{t_1+t_2}^{t_1+t_2+t_3}\mathrm{d}\tau\omega_{10}(\mathbf{Z}^{10,(11,00),10}_{t_1+t_2+\tau})}\rangle_{00} \quad (31)$$

and

$$P^{(3)}_{\mathrm{r}}(t_1,t_2,t_3) = \langle \mu^{10}(\mathbf{Z}_0)\,\mu^{10}(\mathbf{Z}_{t_1})\,\mu^{10}(\mathbf{Z}^{10,00}_{t_1+t_2})\,\mu^{10}(\mathbf{Z}^{10,00,10}_{t_1+t_2+t_3}) \times \mathrm{e}^{i\int_0^{t_1}\mathrm{d}\tau\omega_{10}(\mathbf{Z}^{10}_\tau)-i\int_{t_1+t_2}^{t_1+t_2+t_3}\mathrm{d}\tau\omega_{10}(\mathbf{Z}^{10,00,10}_{t_1+t_2+\tau})}\rangle_{00} + \langle \mu^{10}(\mathbf{Z}_0)\,\mu^{10}(\mathbf{Z}_{t_1})\,\mu^{10}(\mathbf{Z}^{10,(11,11)}_{t_1+t_2})\,\mu^{10}(\mathbf{Z}^{10,(11,11),10}_{t_1+t_2+t_3}) \times \mathrm{e}^{i\int_0^{t_1}\mathrm{d}\tau\omega_{10}(\mathbf{Z}^{10}_\tau)-i\int_{t_1+t_2}^{t_1+t_2+t_3}\mathrm{d}\tau\omega_{10}(\mathbf{Z}^{10,(11,11),10}_{t_1+t_2+\tau})}\rangle_{00} - \langle \mu^{10}(\mathbf{Z}_0)\,\mu^{10}(\mathbf{Z}_{t_1})\,\mu^{10}(\mathbf{Z}^{10,(11,00)}_{t_1+t_2})\,\mu^{10}(\mathbf{Z}^{10,(11,00),10}_{t_1+t_2+t_3}) \times \mathrm{e}^{i\int_0^{t_1}\mathrm{d}\tau\omega_{10}(\mathbf{Z}^{10}_\tau)-i\int_{t_1+t_2}^{t_1+t_2+t_3}\mathrm{d}\tau\omega_{10}(\mathbf{Z}^{10,(11,00),10}_{t_1+t_2+\tau})}\rangle_{00} \quad (32)$$

It should be noted that t_1, t_2, and t_3 should now be interpreted as the time intervals between pulses a and b, pulses b and c, and between pulse c and detection, respectively.

The three terms that contribute to the nonrephasing and rephasing signals in eqs 31 and 32 can be represented diagrammatically as follows:

$$P^{(3)}_{\mathrm{nr}}(t_1,t_2,t_3) = [00 \rightarrow 10 \rightarrow (00 \rightarrow 00) \rightarrow 10] + [00 \rightarrow 10 \rightarrow (11 \rightarrow 11) \rightarrow 10] - [00 \rightarrow 10 \rightarrow (11 \rightarrow 00) \rightarrow 10] \quad (33)$$

$$P^{(3)}_{\mathrm{r}}(t_1,t_2,t_3) = [00 \rightarrow 10 \rightarrow (00 \rightarrow 00) \rightarrow 01] + [00 \rightarrow 10 \rightarrow (11 \rightarrow 11) \rightarrow 01] - [00 \rightarrow 10 \rightarrow (11 \rightarrow 00) \rightarrow 01] \quad (34)$$

This representation can be thought of as a simplified version of Feynman diagrams. The first, second, and last arrows represent transitions between the corresponding populations and coherences induced by the field-matter interactions at times $t = 0$, $t = t_1$, and $t = t_1 + t_2$, respectively. The intermediate section marked by $(\cdots)$ corresponds to the behavior of the Liouville space pathway during t_2. Thus, the first term on the RHS of eqs 33 and 34 corresponds to the Liouville pathway where the system remains in the ground state during t_2, while the second and third terms correspond to the Liouville pathways where the system hops to the excited state (following the first two light-matter interactions). The latter two terms differ however with respect to their behavior during t_2. More specifically, the second (positive) term represents the contribution of trajectories that remain on the excited PES during t_2 (hence $(11 \rightarrow 11)$), while the third (negative) term represents the contribution of trajectories that relax nonradiatively from the excited to the ground PES during t_2 (hence $(11 \rightarrow 00)$).

In the absence of nonadiabatic transitions, the adiabatic result[14] is recovered. More specifically, the Liouville space pathway $[10 \rightarrow (11 \rightarrow 00) \rightarrow 10]$ becomes impossible, while the Liouville space pathway $[10 \rightarrow (11 \rightarrow 11) \rightarrow 10]$ simplifies into $[10 \rightarrow 11 \rightarrow 10]$. Finally, it should be noted that when $t_2 \rightarrow \infty$, the second terms on the RHS of eqs 31 and 32 vanish while the first and third terms become identical and cancel each other out so that the signals vanish. In other words, the lifetime of the signal corresponds to the combined time scales of the nonadiabatic transition and subsequent equilibration on the ground state PES.

The pump−probe signal may be obtained from either eq 31 or eq 32 by setting $t_1 = 0$:

$$P^{(3)}_{\mathrm{pp}}(t_3,t_2) = \langle \mu^{10}(\mathbf{Z}_0)\,\mu^{10}(\mathbf{Z}_0)\,\mu^{10}(\mathbf{Z}^{00}_{t_2})\,\mu^{10}(\mathbf{Z}^{00,10}_{t_2+t_3}) \times \mathrm{e}^{-i\int_{t_2}^{t_2+t_3}\mathrm{d}\tau\omega_{10}(\mathbf{Z}^{00,10}_{t_2+\tau})}\rangle_{00} + \langle \mu^{10}(\mathbf{Z}_0)\,\mu^{10}(\mathbf{Z}_0)\,\mu^{10}(\mathbf{Z}^{(11,11)}_{t_2})\,\mu^{10}(\mathbf{Z}^{(11,11),10}_{t_2+t_3}) \times \mathrm{e}^{-i\int_{t_2}^{t_2+t_3}\mathrm{d}\tau\omega_{10}(\mathbf{Z}^{(11,11),10}_{t_2+\tau})}\rangle_{00} - \langle \mu^{10}(\mathbf{Z}_0)\,\mu^{10}(\mathbf{Z}_0)\,\mu^{10}(\mathbf{Z}^{(11,00)}_{t_2})\,\mu^{10}(\mathbf{Z}^{(11,00),10}_{t_2+t_3}) \times \mathrm{e}^{-i\int_{t_2}^{t_2+t_3}\mathrm{d}\tau\omega_{10}(\mathbf{Z}^{(11,00),10}_{t_2+\tau})}\rangle_{00} \quad (35)$$

The three terms that contribute to the pump−probe signal in eq 35 can be represented diagrammatically as follows:

$$P^{(3)}_{\mathrm{pp}}(t_3,t_2) = [00 \rightarrow (00 \rightarrow 00) \rightarrow 10] + [00 \rightarrow (11 \rightarrow 11) \rightarrow 10] - [00 \rightarrow (11 \rightarrow 00) \rightarrow 10] \quad (36)$$

Finally, we note that the pump−probe spectrum is usually reported in terms of t_2 and ω_3, which is obtained via a Fourier transform with respect to t_3:

$$P_{\mathrm{pp}}(\omega_3,t_2) \equiv \mathrm{Re}\int_0^\infty \mathrm{d}t_3\ \mathrm{e}^{i\omega_3 t_3}P_{\mathrm{pp}}(t_3,t_2) \quad (37)$$

Equation 35 accounts for non-Condon, nonequilibrium, and nonadiabatic effects. It should be noted that although eq 35 corresponds to the pump−probe signal of a two-state system under weak pump and probe fields conditions, it can be easily extended to multistate systems.

The interpretation of the pump−probe signal (eq 35) is facilitated by considering the t_2-dependence of each of the three terms constituting it. We start with the first term, which at time $t_2 = 0$ reduces into

$$\text{term I}\ (t_2 = 0) = \left\langle \left[\mu^{10}(\mathbf{Z}_0)\right]^3 \mu^{10}(\mathbf{Z}^{10}_{t_3})\ \mathrm{e}^{-i\int_0^{t_3}\mathrm{d}\tau\omega_{10}(\mathbf{Z}^{10}_\tau)}\right\rangle_{00} \quad (38)$$

This expression is similar to that of the linear ORF which is given by[14]

$$J(t_3) = \left\langle \mu^{10}(\mathbf{Z}_0)\,\mu^{10}(\mathbf{Z}^{10}_{t_3})\ \mathrm{e}^{-i\int_0^{t_3}\mathrm{d}\tau\omega_{10}(\mathbf{Z}^{10}_\tau)}\right\rangle_{00} \quad (39)$$

The only difference between the two is the extra $[\mu^{10}(\mathbf{Z}_0)]^2$ factor in eq 38, whose main effect is to amplify non-Condon effects by giving more weight to bath configurations that give rise to large transition dipole moments at the expense of bath configurations that give rise to smaller transition

dipole moments. However, since the bath configuration at later times becomes uncorrelated with that at $t_2 = 0$, these non-Condon effects diminish with increasing t_2, asymptotically leading to a signal which is proportional to the linear ORF:

$$\text{term I } (t_2 \to \infty)$$

$$= \left\langle \left[\mu^{10}(\mathbf{Z}_0)\right]^2 \right\rangle_{00} \left\langle \mu^{10}(\mathbf{Z}_0)\, \mu^{10}(\mathbf{Z}_{t_3}^{00,10})\, e^{-i\int_0^{t_3} d\tau \omega_{10}(\mathbf{Z}_\tau^{10})} \right\rangle_{00}$$

$$\equiv \left\langle \left[\mu^{10}(\mathbf{Z}_0)\right]^2 \right\rangle_{00} J(t_3) \tag{40}$$

The time scale on which this process occurs corresponds to that of solvation on the ground state PES.

We next consider the second term in eq 35. At time $t_2 = 0$, this term is identical to the first term (see eq 38), and here too the correlation between the bath configuration at $t_2 = 0$ and that at later times diminishes with increasing t_2. However, in this case the loss of correlation is brought about by solvation on the excited state PES. As a result, the profile of the signal at intermediate values of t_2, which are shorter than the excited state lifetime, is expected to shift toward a profile which is proportional to that of the emission ORF (it should be noted that this implies that correlation with the initial conditions is lost by this time):

$$\left\langle \left[\mu^{10}(\mathbf{Z}_0)\right]^2 \right\rangle \left\langle \mu^{10}(\mathbf{Z}_0)\, \mu^{10}(\mathbf{Z}_{t_3}^{(11,10)})\, e^{-i\int_0^{t_3} d\tau \omega_{10}(\mathbf{Z}_\tau^{(11,10)})} \right\rangle_{11} \tag{41}$$

At values of t_2 equal to or longer than the excited state lifetime, this term diminishes due to nonadiabatic transitions from the excited PES to the ground PES. At the same time, the very same nonadiabatic transitions will give rise to a new contribution to the signal which is represented by the third term in eq 35. This term does not contribute to the signal prior to the occurrence of nonadiabatic transitions. Furthermore, its spectral profile upon emergence is representative of bath configurations where nonadiabatic transitions are most likely to occur. However, since the nonadiabatic transitions are followed by solvation on the ground state PES, this term will eventually have the same spectral profile as the first term and, because it is negative, will cancel out with it, thereby leading to zero overall signal.

IV. H-STRETCH PUMP−PROBE SPECTRA OF A H-BONDED COMPLEX IN A POLAR LIQUID

In this section, we will demonstrate the methodology outlined in the previous section in the case of the H-stretch in a moderately strong H-bonded complex dissolved in a dipolar liquid. This system displays an intricate interplay between nonequilibrium solvation dynamics and nonadiabatic transitions and therefore provides a useful case study.

A. Model and Simulation Techniques. In this subsection, we provide a brief outline of the Azzouz−Borgis (AB) model of a moderately strong H-bonded complex, *AHB*, dissolved in a dipolar liquid (a more detailed description is available in refs 27, 29, 30, and 32). Within this model, it is assumed that the proton moves along a 1D axis connecting the donor and acceptor. The donor, *A*, and acceptor, *B*, are modeled as single particles and parametrized to represent phenol and trimethylamine, respectively. The intramolecular PES as a function of the

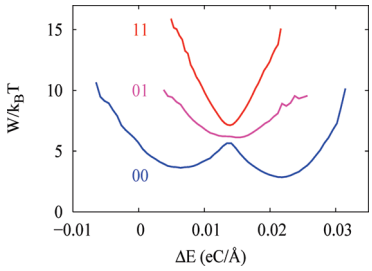

Figure 1. Ground (00, blue) and first-excited (11, red) free energy surfaces as a function of the solvent polarization. Also shown is the averaged free energy surface of the ground and first-excited states (01, magenta).

A−*B* and *A*−*H* distance is the same as that used in refs 29, 33, and 34 with the equilibrium *A*−*B* distance set to 2.7 Å, which corresponds to a moderately strong H-bond. The charges on *A* and *B* are assumed to be explicitly dependent on the position of the proton. The intramolecular PES has a double-well profile as a function of the proton displacement, thereby giving rise to tautomeric equilibrium between covalent and ionic forms: $AH - B \rightleftharpoons A^- - H^+B$.

The solvent is assumed to consist of a liquid of methyl-chloride molecules, which are modeled as rigid dipolar diatomic molecules. The complex−solvent and solvent−solvent interactions are modeled in terms of site−site Lennard−Jones (LJ) and Coulomb interactions, and the corresponding force field parameters are as in refs 29, 33, and 34. Although the covalent form, *AH*−*B*, is favored in the absence of the solvent, the ionic form, A^-H^+B, becomes more stable in the dipolar solvent.

The photoactive quantum DOF is taken to be the high frequency H-stretch, and here we only consider transitions between the ground and the first-excited vibrational states of the H-stretch. The associated transition dipole moment is given by $\boldsymbol{\mu}^{\alpha\beta}(\mathbf{R}) \propto \langle \alpha(\mathbf{R})|\hat{\mathbf{r}}|\beta(\mathbf{R})\rangle$, where $\hat{\mathbf{r}} = \hat{r}\mathbf{u}_{\mathbf{AB}}$ is the position operator corresponding to the H-stretch and $\mathbf{u}_{\mathbf{AB}}$ is the unit vector along the *A*−*B* axis. It should also be noted that the rotational relaxation time is significantly longer than the time scale of the experiment and therefore does not affect the temporal behavior of the signal. The remaining DOF, which constitute the bath, are assumed to be photoinactive and are treated classically. The vibrational energy levels and wave functions are obtained by diagonalizing the adiabatic protonic Hamiltonian on-the-fly using the LAPACK DSYGV routine.[29,33,34]

Molecular dynamics simulations were performed via the velocity Verlet algorithm with a time step of 1 fs. The simulations were performed within a cubic simulation box with periodic boundary conditions, containing a single *AHB* complex and 255 methyl-chloride molecules at a temperature and density of 250 K and 0.012 $Å^{-3}$, respectively. The LJ potentials were spherically truncated at $R_c = 13.8$ Å and shifted accordingly. The Coulomb potentials were smoothly truncated to zero at $R_c = 13.8$ Å.

The pump−probe signal was calculated based on eq 35 by averaging over 16 000 nonequilibrium trajectories for each point on a t_3 time grid with $0 < t_3 < 250$ fs (time interval of 1 fs) for various values of t_2. The 250-point time grid was then padded with zeros to generate a 2048-point time grid. The 1D Fourier transform required for computing the pump−probe spectrum, eq 37, was carried out numerically via the FFT routine.

B. Free Energy Surfaces and Transition Frequencies. The pump−probe spectra reported below directly probe the

dx.doi.org/10.1021/jp1061495 |J. Phys. Chem. B 2011, 115, 5191–5200

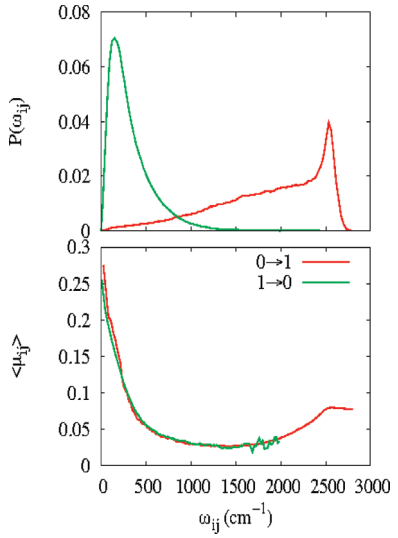

Figure 2. Upper panel: The distributions of the fundamental transition frequency, ω_{10}, corresponding to equilibrium on the ground state PES (red) and first-excited state PES (green). Lower panel: The average transition dipole moment, μ_{10}, as a function of the transition frequency, ω_{10}, at equilibrium on the ground state PES (red) and first-excited state PES (green).

transitions between the ground and first-excited state of the H-stretch. The corresponding vibrational energy levels and wave functions follow the bath DOF adiabatically and are therefore explicitly dependent on the bath coordinates. It is convenient to consider this dependence in terms of a collective order parameter, such as the solvent polarization, ΔE, which is defined as the difference between the solvent electrical potentials at the minima of the covalent and ionic wells.[27,29,30] Figure 1 shows the ground (00) and first-excited (11) free energy surfaces (FESs), as well as the average of the ground and first-excited state FES (01), as a function of the solvent polarization. The fact that the FESs are very different suggests that the same is true for the corresponding multidimensional PESs, and serves as an indication for the strong coupling between the H-stretch and the bath.

The ground state FES is seen to have a double-well profile, which reflects coexistence between the ionic and covalent tautomers (equilibrium composition: 65% ionic and 35% covalent; proton transfer rate constant: 0.16 ps^{-1}).[30] In contrast, the first-excited FES has the shape of a symmetric single well whose minimum is centered in the vicinity of the ground state transition-state between the ionic and covalent tautomers. It is important to note that the ionic/covalent tautomers and transition-state correspond to stable and unstable solvent configurations, respectively, when the chromophore is in its ground state. In contrast, the ionic/covalent tautomers and transition-state correspond to unstable and stable solvent configurations, respectively, when the chromophore is in its first-excited state.

The rather small transition frequency in the vicinity of the transition state (see Figure 1) suggests a high likelihood for nonadiabatic transitions in this region. This, in turn, implies that one can expect significant signatures of nonradiative nonadiabatic dynamics on the pump−probe IR spectra of the H-stretch, thereby making this an appropriate model system for exploring these effects. Moreover, the pronounced differences between the FESs suggest that any transition (radiative or nonradiative) between them will be accompanied by a similarly pronounced solvent reorganization. In ref 14, we showed how these differences gave rise to notable signatures of nonequilibrium dynamics on the 1D- and 2D-IR spectra of the H-stretch.

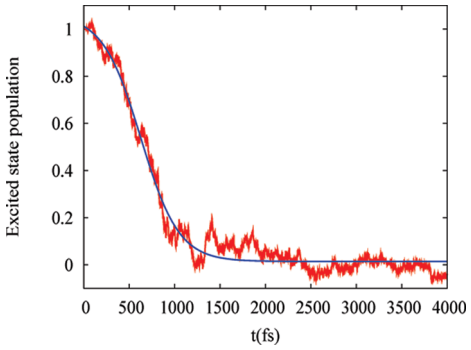

Figure 3. Nonadiabatic relaxation of the excited-state population, as obtained via the MQCL method when the initial ensemble of bath configurations corresponds to equilibrium on the ground-state PES (red curve).[29] A fit to this decay based on eq 42 is shown in blue.

Finally, in the upper panel of Figure 2, we show the distributions of the fundamental transition frequency, ω_{10}, that correspond to equilibrium on the ground state PES (red) and first-excited state PES (green). The transition frequency distributions are seen to be rather broad and pronouncedly different in range and in shape, all of which are manifestations of the strong coupling between the H-stretch and the bath. In the lower panel of Figure 2, we show the dependence of the fundamental transition dipole moment, $\mu_{10}(\mathbf{Z})$, averaged over all the configurations that correspond to a given value of the transition frequency, on the fundamental transition frequency, ω_{10}, at equilibrium on the ground state PES (red) and first-excited state PES (green). The rather dramatic enhancement of the transition dipole moments in the low frequency region reflects the great sensitivity of the adiabatic state wave functions to the configuration of the bath in this region, which in turn gives rise to very pronounced non-Condon effects in this system.[33]

C. Nonadiabatic Transitions. As discussed in section III, nonadiabatic transitions can be described as occurring directly between 11 and 00. To this end, we can employ the 11 state population relaxation profile previously reported in ref 29 (see Figure 3), which was calculated by solving the MQCL equation (eq 7). It should be noted that impulsive photoexcitation is typically followed by solvation on the excited state PES during which the transition frequency decreases thereby making nonadiabatic transitions more likely. As a result, the relaxation profile of the 11 population is distinctly nonexponential and can be fit with the following functional form (see Figure 3):

$$P(t) = a + \frac{b-a}{1+\mathrm{e}^{(t-x_0)/\mathrm{d}x}} \tag{42}$$

where $a = 0.01444$, $b = 1.06096$, $x_0 = 628.36824$ fs, and $\mathrm{d}x = 208.89635$ fs. $P(t)$ corresponds to the distribution of time intervals between photoexcitation and the occurrence of a nonadiabatic transition. In practice, we treat t as a random variable which can be sampled based on the probability given by eq 42. To this end, we sample a uniform random number ξ between (0, 1), and obtain the corresponding value of t via the following relation:

$$t = P^{-1}(\xi) = \mathrm{d}x \ln\left(\frac{b-a}{\xi-a} - 1\right) + x_0 \tag{43}$$

dx.doi.org/10.1021/jp1061495 |J. Phys. Chem. B 2011, 115, 5191–5200

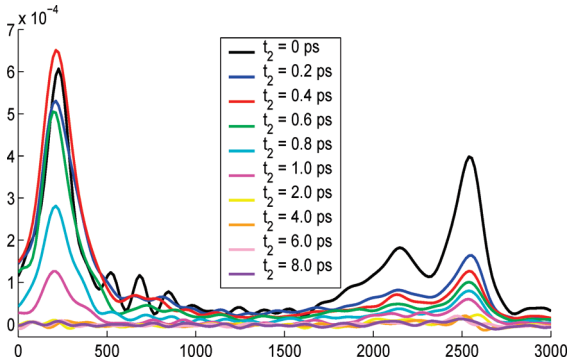

Figure 4. Overall pump−probe IR spectra of the H-stretch calculated based on eq 35 for various values of t_2 ranging from 0 to 8 ps.

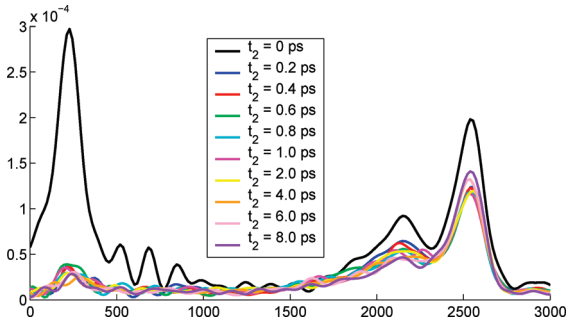

Figure 5. Contribution of the first term in eq 35 to the pump−probe spectrum as a function of t_2.

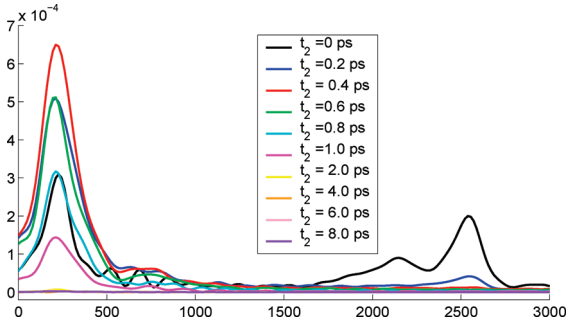

Figure 6. Contribution of the second term in eq 35 to the pump−probe spectrum as a function of t_2.

where P^{-1} denotes the inverse function. Finally, the nonadiabatic transition is accompanied by an instantaneous shift to the bath momenta according to the momentum jump approximation:[27]

$$\Delta \mathbf{P} = M^{1/2}\left\{ \mathrm{sgn}(\hat{\bar{\mathbf{d}}}_{10}\cdot\bar{\mathbf{P}})\sqrt{(\hat{\bar{\mathbf{d}}}_{10}\cdot\bar{\mathbf{P}})^2 + 2\Delta E_{10}} - (\hat{\bar{\mathbf{d}}}_{10}\cdot\bar{\mathbf{P}}) \right\}\hat{\bar{\mathbf{d}}}_{10} \tag{44}$$

where $M^{1/2}$ is a diagonal matrix with $(M_j)^{1/2}$ along the diagonal, $\bar{P}_j = P_j/(M_j)^{1/2}$, $\bar{d}_{10,j} = d_{10,j}/(M_j)^{1/2}$, and $\hat{\bar{\mathbf{d}}}_{\alpha\beta} = \bar{\mathbf{d}}_{\alpha\beta}/|\bar{\mathbf{d}}_{\alpha\beta}|$ is a unit vector along $\bar{\mathbf{d}}_{\alpha\beta}$. It should be noted that the factor of 2 in front of ΔE_{10} accounts for the fact that the nonadiabatic transition from the excited PES to the ground PES corresponds to two sequential MQCL transitions: one from the excited PES to the average PES and the other from the average PES to the ground PES.

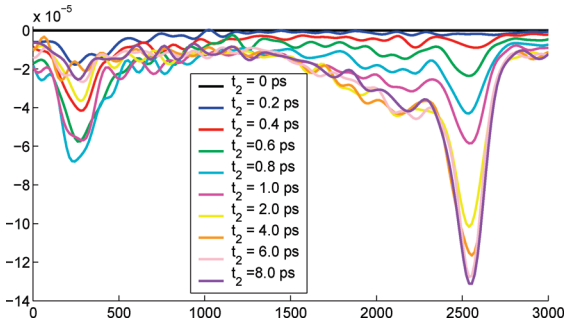

Figure 7. Contribution of the third term in eq 35 to the pump−probe spectrum as a function of t_2.

D. Pump−Probe Spectra. The pump−probe IR spectra of the H-stretch calculated using eq 37 for various values of t_2 ranging from 0 to 8 ps are shown in Figure 4. The three terms that contribute to the pump−probe signal are shown separately in Figures 5−7, in the order of their appearance in eq 35.

The *first term* is seen to consist of three bands centered at ∼200, ∼2200, and ∼2500 cm^{-1}, which have been previously assigned to the transition state, covalent, and ionic bath configurations, respectively (see Figure 5).[33] The lack of absorption in the intermediate frequency region and the emergence of the low frequency transition state band can be traced back to non-Condon effects. More specifically, they are due to the fact that the transition dipole moments are small in the intermediate frequency region and large in the low frequency region (see lower panel of Figure 2). As discussed previously, the extra $[\mu^{10}(\mathbf{Z}_0)]^2$ factor in eq 38 (in comparison to the linear response ORF, eq 39) enhances the non-Condon effects so that the transition-state peak at $t_2 = 0$ is significantly more pronounced in comparison to the corresponding peak in the absorption spectrum.[14] However, as expected, the spectral profile that arises from this term reduces to that of the absorption spectrum on a time scale of ∼0.2 ps due to solvation on the ground state PES. Thus, the main effect of ground state solvation on the first term is to diminish the transition state peak relative to the ionic and covalent peaks. Importantly, this term does not change significantly for $t_2 > 0.2$ ps.

As previously discussed, the *second term* is seen to coincide with the first term at $t_2 = 0$ (see Figure 6). However, in contrast to the first term, the transition state peak is seen to intensify with increasing t_2 at the expense of the ionic and covalent peaks. This behavior can be traced back to solvation dynamics on the excited state PES where the transition state configurations are stable while the ionic and covalent ones are not. Indeed, at the end of this solvation process ($t_2 \sim 0.5$ ps), the spectral profile of this term coincides with that of the emission spectrum, which consists of one major low frequency peak due to bath configurations that correspond to the transition state on the ground state PES (see upper panel of Figure 2). However, the fact that solvation on the excited state PES reduces the transition frequency also makes nonadiabatic transitions more likely. These nonadiabatic transitions then diminish the signal that arise from the second term at $t_2 > 0.5$ ps until it disappears completely by $t_2 \sim 2.0$ ps, signaling the completion of the population relaxation process from the excited to the ground state.

As expected, the disappearance of the contribution to the signal that arises from the second term is accompanied by the emergence of a contribution to the signal that arises from the third term (see Figure 7). The latter is seen to emerge at $t_2 \sim 0.4$ ps with a spectral

dx.doi.org/10.1021/jp1061495 |J. Phys. Chem. B 2011, 115, 5191–5200

profile similar to that of the emission spectrum and therefore dominated by the low frequency transition state peak. However, solvation on the ground state PES is seen to shift the spectral profile of this term toward that of the absorption spectrum which is dominated by the higher frequency ionic and covalent peaks. It should be noted that complete equilibration on the ground state PES takes about 8 ps and is much longer than the corresponding process on the excited PES. The rate determining step in this case is the tautomerization reaction that interchanges between the ionic and covalent species and requires crossing a significant free energy barrier. Indeed, initially ($0 < t_2 < 0.5$ ps), the intensities of the ionic and covalent peaks appear to be similar, but at longer times the ionic peak becomes more intense because of equilibration via proton transfer between the ionic and covalent species and the fact that the ionic species has a stronger transition dipole moment than the covalent species (see Figure 2).

Upon summation of the three terms, it is seen that the overall signal vanishes by the time $t_2 = 2$ ps (see Figure 4), which can be traced back to the disappearance of the second term due to nonadiabatic transitions, and the fact that the first and third terms practically cancel each other out due to ground state solvation.

V. CONCLUDING REMARKS

In this paper, we presented a general formulation of the third-order ORF within the framework of the MQCL equation. The temporal behavior of the ORF within this formulation is seen to reflect nonequilibrium solvation dynamics on multiple PESs as well as nonadiabatic transitions. More specifically, the photo-inactive DOF undergo transitions between the adiabatic PESs and their averages caused by either light-matter interactions or nonadiabatic coupling. This should be contrasted with the standard approach, which involves ORFs that reflect equilibrium dynamics that takes place solely on the ground state PES.

The feasibility and usefulness of this approach were demonstrated on the Azzouz−Borgis model of a moderately strong H-bonded complex dissolved in a dipolar liquid. Nonadiabatic transitions were shown to have a pronounced effect on the pump−probe IR spectra of the H-stretch in this rather nontrivial model system. As a result, these spectra were seen to provide a wealth of detailed information on the interplay between solvation dynamics on multiple PESs and nonadiabatic transitions between them, which are known to dominate photochemistry.

Generally speaking, the methodology presented herein should be particularly useful in strongly coupled systems such as the H-stretch in H-bonded liquids. In these systems, one should expect the pump−probe spectra to reflect the nonequilibrium dynamics of the underlying H-bonded network as it is disrupted by solvation processes and nonadiabatic transitions. The investigation of these aspects in the case of systems for which experimental spectra are available is underway in our group and will be presented in future publications.

AUTHOR INFORMATION

Corresponding Author

* E-mail: gabriel.hanna@ualberta.ca, eitan@umich.edu.

ACKNOWLEDGMENT

This work was supported by the National Science Foundation through Grant CHE-0809506.

REFERENCES

(1) Mukamel, S. *Principles of Nonlinear Optical Spectroscopy*; Oxford: New York, 1995.
(2) Fleming, G. R.; Cho, M. *Annu. Rev. Phys. Chem.* **1996**, *47*, 109.
(3) Joo, T.; Jia, Y.; Yu, J.; Lang, M. J.; Fleming, G. R. *J. Chem. Phys.* **1996**, *104*, 6089.
(4) Jonas, D. M. *Annu. Rev. Phys. Chem.* **2003**, *54*, 425.
(5) Khalil, M.; Demirodoven, N.; Tokmakoff, A. *J. Phys. Chem. A* **2003**, *107*, 5258.
(6) Cho, M. *Chem. Rev.* **2008**, *108*, 1331.
(7) Ogilvie, J. P.; Kubarych, K. J. *Adv. At., Mol., Opt. Phys.* **2009**, *57*, 249–321.
(8) McRobbie, P. L.; Geva, E. *J. Phys. Chem. A* **2009**, *113*, 10425.
(9) McRobbie, P. L.; Hanna, G.; Shi, Q.; Geva, E. *Acc. Chem. Res.* **2009**, *42*, 1299.
(10) Shi, Q.; Geva, E. *J. Chem. Phys.* **2008**, *129*, 124505.
(11) Skinner, J. L. *J. Chem. Phys.* **1982**, *77*, 3398.
(12) Mukamel, S. *J. Chem. Phys.* **1982**, *77*, 173.
(13) Walsh, A. M.; Loring, R. F. *Chem. Phys. Lett.* **1991**, *186*, 77.
(14) Hanna, G.; Geva, E. *J. Phys. Chem. B* **2009**, *113*, 9278.
(15) Martens, C. C.; Fang, J. *J. Chem. Phys.* **1997**, *106*, 4918.
(16) Donoso, A.; Martens, C. C. *J. Chem. Phys.* **1998**, *102*, 4291.
(17) Donoso, A.; Martens, C. C. *J. Chem. Phys.* **2000**, *112*, 3980.
(18) Donoso, A.; Kohen, D.; Martens, C. C. *J. Chem. Phys.* **2000**, *112*, 7345.
(19) Schütte, C. *Konard-Zuse-Zentrum für informationstechnik Berlin*, June 1999, pages Preprint SC 99−10.
(20) Santer, M.; Manthe, U.; Stock, G. *J. Chem. Phys.* **2001**, *114*, 2001.
(21) Kapral, R.; Ciccotti, G. *J. Chem. Phys.* **1999**, *110*, 8919.
(22) Nielsen, S.; Kapral, R.; Ciccotti, G. *J. Chem. Phys.* **2000**, *112*, 6543.
(23) Wan, C.; Schofield, J. *J. Chem. Phys.* **2000**, *113*, 7047.
(24) Wan, C.; Schofield, J. *J. Chem. Phys.* **2000**, *112*, 4447.
(25) Kapral, R. *Annu. Rev. Phys. Chem.* **2006**, *57*, 129.
(26) Shi, Q.; Geva, E. *J. Chem. Phys.* **2004**, *121*, 3393.
(27) Hanna, G.; Kapral, R. *J. Chem. Phys.* **2005**, *122*, 244505.
(28) Hanna, G.; Kapral, R. *Acc. Chem. Res.* **2006**, *39*, 21.
(29) Hanna, G.; Geva, E. *J. Phys. Chem. B* **2008**, *112*, 4048.
(30) Hanna, G.; Kapral, R. *J. Chem. Phys.* **2008**, *128*, 164520.
(31) Shi, Q.; Geva, E. *J. Chem. Phys.* **2005**, *122*, No. 064506.
(32) Azzouz, H.; Borgis, D. *J. Chem. Phys.* **1993**, *98*, 7361.
(33) Hanna, G.; Geva, E. *J. Phys. Chem. B* **2008**, *112*, 12991.
(34) Hanna, G.; Geva, E. *J. Phys. Chem. B* **2008**, *112*, 15793.